CELL BIOLOGY

The cohesin release factor Wapl interacts with Bub3 to govern SAC activity in female meiosis I

Changyin Zhou, Yilong Miao, Zhaokang Cui, Xiayan ShiYang, Yu Zhang, Bo Xiong*

During mitotic prophase, cohesins are removed from chromosome arms by Wapl to ensure faithful sister chromatid separation. However, during female meiosis I, the resolution of chiasmata requires the proteolytic cleavage of cohesin subunit Rec8 along chromosome arms by Separase to separate homologs, and thus the role of Wapl remained unknown. Here, we report that Wapl functions as a regulator of spindle assembly checkpoint (SAC) to prevent aneuploidy in meiosis I. Depletion of Wapl accelerates meiotic progression, inactivates SAC, and causes meiotic defects such as aberrant spindle/chromosome structure and incorrect kinetochore-microtubule (K-MT) attachment, consequently leading to aneuploid eggs. Notably, we identify Bub3 as a binding partner of Wapl by immunoprecipitation and mass spectrometry analysis. We further determine that Wapl controls the SAC activity by maintaining Bub3 protein level and document that exogenous Bub3 restores the normal meiosis in Wapl-depleted oocytes. Together, our findings uncover unique, noncanonical roles for Wapl in mediating control of the SAC in female meiosis I.

INTRODUCTION

Sister chromatid cohesion, indispensable for a variety of biological processes that occur on chromosomes such as chromosome segregation, double-strand break repair, and gene expression, is mediated by a cohesin complex that is composed of four core components arranged in a ring-shaped structure (*1*–*3*). Two of the subunits are SMC (structural maintenance of chromosomes) proteins, Smc1 and Smc3; one is a kleisin subunit Mcd1 (Scc1/Rad21); and the fourth subunit is Scc3/stromal antigen (SA/STAG) (*4*). In addition, the association of the cohesin complex with chromatin is controlled by several regulatory factors over the cell cycle. In telophase (vertebrates), cohesin loads onto chromatin with the help of the Nipbl-Mau2 heterodimer (*5*). During S phase, the Smc3 subunit of cohesin is acetylated on by acetyltransferases Esco1 and Esco2 to establish sister chromatid cohesion (*6*). Sororin is then recruited to Pds5 to antagonize Wapl (wings apart-like protein) function and stabilize cohesin on sister chromatids (*7*). During prophase, binding of Wapl to Pds5 displaces phosphorylated Sororin and remove a bulk of cohesin complexes from chromosome arms (*8*). However, centromeric cohesin is protected from removal by Sgo1 (shugoshin 1) and Pp2A (protein phosphatase 2A) by antagonizing Sororin phosphorylation (*9*). At the onset of anaphase, the APC/C (anaphase-promoting complex/cyclosome) complex activates Separase to cleave the kleisin subunit, which releases centromeric cohesin and separates sister chromatids (*10*).

As a cohesin release factor, Wapl is indispensable for mitotic progression and depletion of Wapl delays early stages of the cell cycle (*11*, *12*). Moreover, *Wapl* expression is required for mammalian embryonic development and homozygous null mice are embryonic lethal (*13*). Meiosis, unlike mitosis, serves to generate haploid gametes from diploid precursors, as the two successive divisions (known as meiosis I and meiosis II) occur with only one round of DNA replication. Meiosis I is unique in that homologous chromosomes (bivalents) separate from each other (*14*). The distinct roles of Wapl in regulating chromosome during meiosis have been recently reported in multiple organisms. In plants, Wapl removes cohesin before metaphase in both meiosis and mitosis (*15*), and in budding yeast, Wpl1 (Wapl homolog) participates in synaptonemal complex formation, telomere dynamics, and meiotic recombination (*16*). In *Caenorhabditis elegans*, Wapl-1 regulates meiotic chromosome structure and a Wapl-1–independent mechanism removes cohesin before metaphase I during oocyte maturation (*17*). In mammals, Wapl is present on the meiotic chromosome cores in both male and female germ cells (*18*, *19*). In mouse spermatocytes, Nek1 phosphorylates Pp1γ, leading to the dephosphorylation of Wapl, which, in turn, results in its retention on chromosome cores to promote loss of cohesion at the end of prophase I (*20*). However, the exact function of Wapl during oocyte meiosis I in mammals has lacked clarity. We now report a noncanonical role of Wapl in mediating the spindle assembly checkpoint (SAC) by interacting with Bub3 during female meiosis I.

RESULTS

Subcellular localization and expression of Wapl during oocyte meiosis

To investigate the potential role of Wapl during meiotic maturation, we first examined its subcellular localization in mouse oocytes. We microinjected Wapl–green fluorescent protein (GFP) mRNA into germinal vesicle (GV) oocytes and confirmed by immunoblot that the levels of Wapl-GFP protein were comparable to endogenous Wapl (fig. S1A). Fluorescent images showed that Wapl was primarily present in the GV (nucleus) at the GV stage of oocyte development. After GVBD (GV breakdown), Wapl was concentrated on chromosomes at prometaphase I, metaphase I, anaphase I/telophase I, and metaphase II stages (Fig. 1A). GFP mRNA, injected as a negative control, was evenly distributed in the cytoplasm (fig. S1B). The immunostaining of chromosome spreads with antibody revealed that endogenous Wapl was also localized on the chromosomes, but unanticipatedly displayed a strong accumulation staining at kinetochores (Fig. 1B). The localization of Wapl during meiosis differs from mitosis where it is detected in the nucleus during interphase and late telophase, but not present on chromosomes from prometaphase to anaphase in HeLa cells (*12*).

We next assessed protein accumulation of Wapl during oocyte meiosis. Oocytes collected from GV, prometaphase I, metaphase I,

College of Animal Science and Technology, Nanjing Agricultural University, Nanjing 210095, China.
*Corresponding author. Email: xiongbo@njau.edu.cn

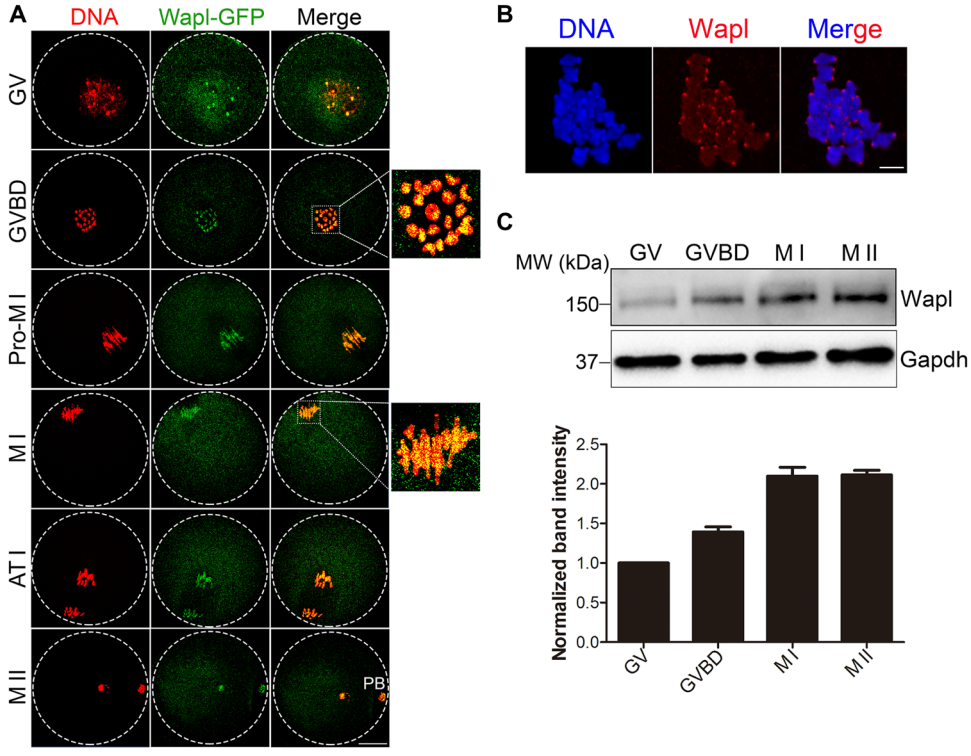

Fig. 1. Meiotic dynamics of Wapl in mouse oocytes. (**A**) Representative images of Wapl-GFP localization during mouse oocyte meiosis. Mouse oocytes were microinjected with Wapl-GFP mRNA at GV stage, maintained for 2 hours in 2.5 μM milrinone before being washed into milrinone-free medium to allow development to GVBD, Pro-M I, M I, AT I, and M II stages, followed by DNA staining with propidium iodide (PI). Scale bar, 20 μm. (**B**) Representative images of the localization of endogenous Wapl in oocytes. Oocytes were immunostained for Wapl following chromosome spreading. Scale bar, 5 μm. (**C**) Protein levels of Wapl during oocyte meiosis corresponding to GV (0 hour), GVBD (4 hours), M I (8 hours), and M II (12 hours) stages were examined by immunoblot. The blots were probed with anti-Wapl antibody and anti-Gapdh antibody. The band intensity of Wapl was normalized with that of Gapdh. Data were presented as mean value (mean ± SEM) of three independent experiments.

and metaphase II stages were analyzed by immunoblots using Wapl antibody. These results documented that Wapl was robustly up-regulated from prophase I to metaphase II stages in oocytes (Fig. 1C and fig. S1C), whereas in marked contrast, the abundance of Wapl protein was relatively constant throughout the cell cycle in HeLa cells (*12*). Together, the differences noted in meiotic and mitotic cell cycle dynamics suggests that Wapl might have distinct functions in oocyte meiosis.

Depletion of Wapl accelerates meiotic progression and inactivates the SAC

To explore the role of Wapl in oocyte meiosis, loss-of-function experiments with gene-targeting morpholinos were performed in oocytes. More than 70% of the targeted protein was down-regulated in Wapl-depleted oocytes as judged by immunoblot (Fig. 2A and fig. S2A). This decrease of Wapl abundance in the morpholino-based silencing approach was comparable to that of small interfering RNA (siRNA)–mediated gene silencing (fig. S2B) and confirmed by the immunostaining analysis, showing that Wapl signals at both chromosomes and kinetochores were remarkably reduced in Wapl-depleted oocytes (fig. S2C). To assess the effect of Wapl depletion on meiotic progression, we recorded the frequency of GVBD and PBE (polar body extrusion), two critical developmental events during oocyte meiosis. We found that depletion of Wapl did not significantly affect GVBD (Fig. 2B), but unexpectedly, there was a considerably higher incidence of PBE observed in Wapl-depleted oocytes than in control oocytes at the time point of 6 and 7 hours after GVBD (Fig. 2, C and D). The final rate of PBE at 10 hours after GVBD was comparable between the two groups (Fig. 2D), indicating that meiotic progression was accelerated in the absence of Wapl. To rule out the possibility that premature PBE was due to off-target effects of the morpholinos, we expressed exogenous Wapl in Wapl-depleted oocytes to monitor meiotic progression. The recovery of Wapl protein level in Wapl-rescue oocytes was confirmed by immunoblot (fig. S2D). As anticipated in the rescued oocytes, the frequency of PBE at 6 and 7 hours after GVBD was reduced to a level indistinguishable from controls (Fig. 2D). This PBE kinetics was recapitulated by knocking down Wapl with siRNA and rescuing with siRNA-resistant Wapl mRNA (fig. S2E).

The precocious PBE implies that the SAC activity might be compromised. We observed similar kinetics of accelerated PBE when the SAC was inhibited with Mps1 inhibitor reversine (fig. S2F), although the timing of PBE was even earlier than observed with Wapl depletion. This observation was further validated by the change of Securin protein levels at different time points during meiotic progression (fig. S2G). Another line of evidence to substantiate impaired SAC function in Wapl-depleted oocytes is that they were able to override the M I arrest induced by nocodazole, unlike control and Wapl-rescue oocytes (Fig. 2E). In addition, BubR1, a crucial part of the SAC complex, was immunostained in oocytes as an indicator (*21*, *22*). As shown in Fig. 2 (F to H) and fig. S2 (H to J), BubR1 was recruited to the unattached kinetochores at prometaphase I

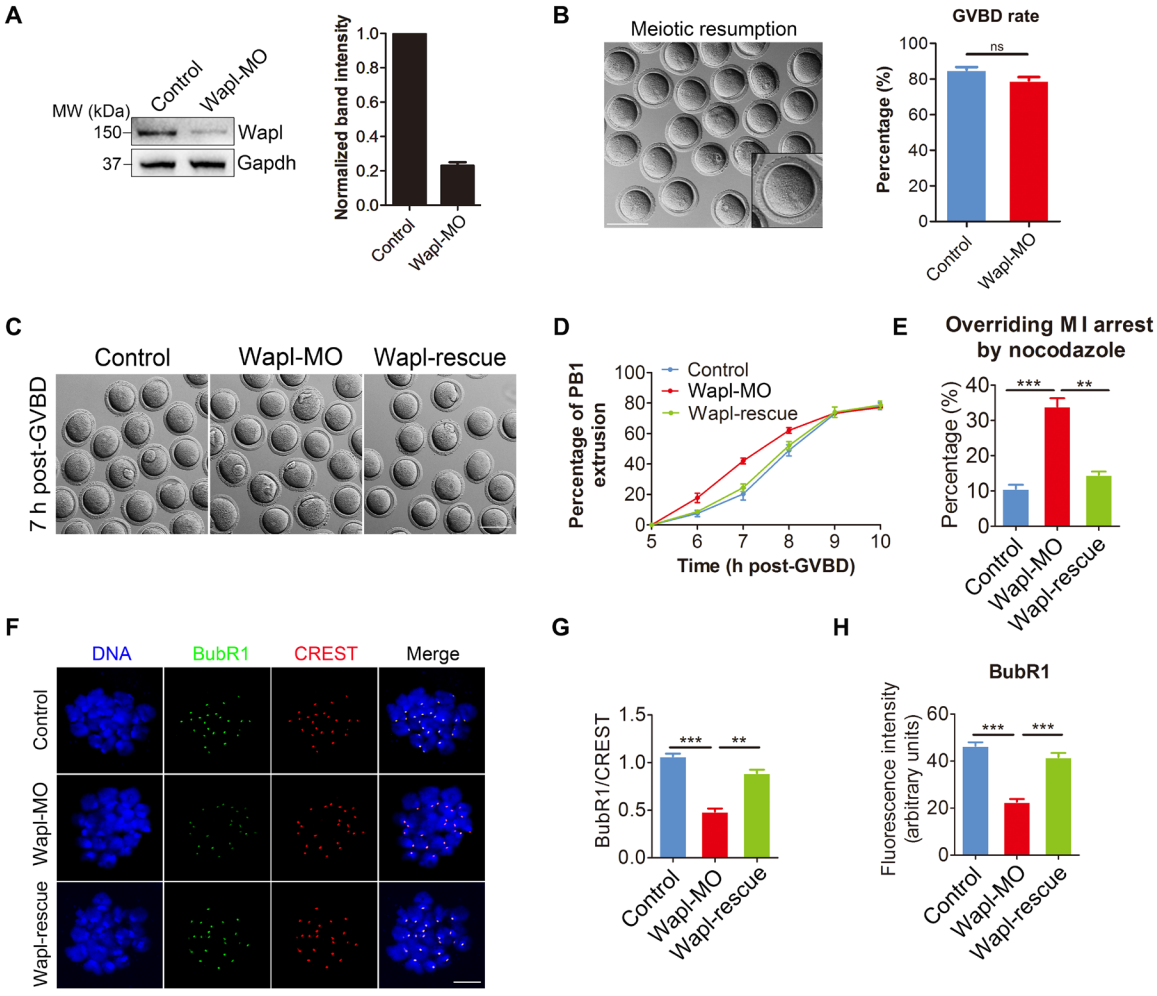

Fig. 2. Effect of Wapl depletion on meiotic progression and the SAC activity in mouse oocytes. (**A**) Knockdown efficiency of Wapl by injection of morpholino was tested in control and Wapl-MO (morpholino) oocytes by immunoblots. GV oocytes were injected with control or Wapl-specific morpholinos, maintained for 20 hours in 2.5 μM milrinone to inhibit mRNA translation. Then, 200 oocytes for each group were collected and immunoblotted for Wapl and Gapdh. The band intensity of Wapl was normalized with that of Gapdh. (**B**) Wapl depletion has no effect on the occurrence of GVBD. Quantitative analysis of GVBD rate was shown in control ($n = 165$) and Wapl-MO ($n = 152$) oocytes, accompanied by the representative images of meiotic resumption in Wapl-MO oocytes. Scale bar, 100 μm. (**C**) Representative images of PBE in control, Wapl-MO, and Wapl-rescue oocytes at 7 hours after GVBD. Scale bar, 100 μm. (**D**) Quantitative analysis of PBE rate was shown in control ($n = 135$), Wapl-MO ($n = 128$), and Wapl-rescue ($n = 148$) oocytes at consecutive time points after GVBD. For the rescue experiments, GV oocytes were injected with Wapl-specific morpholino and maintained for 20 hours in 2.5 μM milrinone before being injected with morpholino-resistant Wapl mRNA and maintained for a further 2 hours in 2.5 μM milrinone to allow time for Wapl translation. Oocytes were then washed into milrinone-free medium to allow resumption of meiosis. (**E**) The proportion of oocytes overriding metaphase I arrest by nocodazole treatment was recorded in control ($n = 98$), Wapl-MO ($n = 95$), and Wapl-rescue ($n = 92$) oocytes. Oocytes injected with the indicated morpholino and/or mRNA were cultured with 400 nM nocodazole from 4 hours after GVBD, and the PBE rate was scored at 10 hours after GVBD. (**F**) SAC activity was indicated by the localization of BubR1 at prometaphase I stage in control, Wapl-MO, and Wapl-rescue oocytes. At 3 hours after GVBD, oocytes were fixed and immunostained for BubR1, CREST, and DNA (Hoechst). Scale bar, 10 μm. (**G**) The relative fluorescence intensity of BubR1 to CREST was measured in control ($n = 182$), Wapl-MO ($n = 191$), and Wapl-rescue ($n = 188$) oocytes. The signal intensity of BubR1 was normalized with that of CREST. (**H**) The fluorescence intensity of BubR1 was measured in control ($n = 182$), Wapl-MO ($n = 191$), and Wapl-rescue ($n = 188$) oocytes. Data of (B), (D), (E), (G), and (H) were presented as mean percentage or value (mean ± SEM) of at least three independent experiments. $^{**}P < 0.01$, $^{***}P < 0.001$. ns, not significant.

stage in control oocytes. However, about 50% of BubR1 was lost from kinetochores in Wapl-depleted oocytes, indicating that Wapl depletion impairs the SAC complex and activity.

Collectively, our findings suggest that Wapl is implicated in control of the SAC activity and orchestrates meiotic progression that differs from observations in mitosis in which depletion of Wapl causes prometaphase delay but does not affect progression from prometaphase through anaphase (*12*).

Depletion of Wapl causes meiotic spindle defects, chromosome misalignment, and aneuploidy

Given its participation in the SAC control during oocyte meiosis, we hypothesized that Wapl might play a regulatory role in spindle assembly and chromosome alignment. After staining, more than 80% of control oocytes displayed a typical barrel-shaped spindle with well-aligned chromosomes on the metaphase plate (Fig. 3, A, B, and D). Depletion of Wapl frequently resulted in spindle assembly defects

(Fig. 3, A and B) and failed chromosome alignment (Fig. 3, A and D). These defects include a variety of apolar, elongated, and multipolar spindles with one or several scattered or lagging chromosomes, which did not realign even at anaphase I stage (Fig. 3, A and C, and fig. S3, A and B). Notably, spindle defects in Wapl-depleted oocytes could be rescued by expression of exogenous Wapl (fig. S3, C and D). Furthermore, the width of the chromosome plate at M I stage was considerably wider in Wapl-depleted than in control oocytes (Fig. 3, E and F). A similar phenotype with altered spindle length and M I chromosome plate width was observed when the SAC was inactivated with Mps1 inhibitor reversine (fig. S3, E to G).

The remarkably higher occurrence of misaligned chromosomes in Wapl-depleted oocytes suggested impairment of kinetochore-microtubule (K-MT) attachments. Therefore, oocytes were cold-treated to induce depolymerization of microtubules that are not attached to kinetochores. In control oocytes, we observed that microtubules mostly captured the kinetochores on the aligned bivalents at the equator (Fig. 3, G and H). Conversely, we detected a higher frequency of unattached kinetochores with few cold-stable microtubules in Wapl-depleted oocytes (Fig. 3, G and H). These observations suggest that Wapl is required for proper K-MT attachments in meiosis.

Incorrect or unstable K-MT attachments contribute to bivalent misalignment and discordant divisions, which cause aneuploidy in mammalian eggs (*23*, *24*). In karyotyping control oocytes, we found that a large majority were euploid and had the correct number of univalents (Fig. 3I). However, the incidence of hyperploidy (>20 univalents) in Wapl-depleted oocytes increased from ~3% in control oocytes to 15% and decreased to roughly 5% after expressing exogenous Wapl (Fig. 3, I and J). Similar defects in spindle/chromosome structure resulting in aneuploidy were observed in oocytes after depletion of Wapl by siRNA (fig. S4).

Depletion of Wapl does not affect chromosome cohesion during oocyte meiosis I

To determine whether the chromosome defects and aneuploidy in Wapl-depleted oocytes was due to the compromised chromosome cohesion, we assessed the binding of cohesin to chromosomes by immunostaining for two subunits of cohesion, Rec8 and Smc3 (Fig. 4, A and C). The fluorescence intensity was indistinguishable from controls (Fig. 4, B and D), indicating that Wapl depletion does not affect cohesin binding. This was further confirmed by immunoblots that the abundance of Rec8 and Smc3 proteins was not altered in Wapl-depleted oocytes (Fig. 4, E and F). In addition, Wapl depletion did not influence the morphology of bivalents and the distance separating the two sister kinetochore pairs within a bivalent (Fig. 4, G and H). These observations suggest that Wapl is essential for maintenance of euploidy by modulating spindle and chromosome dynamics independent of chromosome cohesion during oocyte meiosis I.

Wapl interacts with Bub3 and is required for its protein levels

To gain insight into the molecular function of Wapl in the control of SAC activity, we used immunoprecipitation and mass spectrometry (MS) to identify its potential downstream effectors. Among the candidates, we found that Bub3, a conserved SAC component in both mitosis and meiosis (*25*), is a binding partner of Wapl (Fig. 5A and data S1). We verified the interaction between Wapl and Bub3 by performing co-immunoprecipitation (co-IP) experiments in oocytes and human embryonic kidney (HEK) 293 cells (Fig. 5, B to D). In addition, we costained Wapl and Bub3 in oocytes and observed that Bub3 colocalized with Wapl at kinetochore regions (Fig. 5E).

To determine whether Bub3 is a downstream effector of Wapl in the SAC control, we examined the localization and expression of Bub3 in Wapl-depleted oocytes. Immunostaining documented that Wapl depletion by targeted morpholino or siRNA did not change the localization of Bub3 at kinetochores. However, the fluorescent signal was remarkably reduced (Fig. 5, F to H, and fig. S5, A to F), and immunoblotting confirmed that the protein level of Bub3 was significantly decreased in Wapl-depleted oocytes (Fig. 5I and fig. S5, G and H). As expected, reduced levels of Bub3 could be restored by expressing exogenous Wapl in Wapl-depleted oocytes as judged by immunostaining and immunoblots (Fig. 5, F to I, and fig. S5). Using similar approaches, we assessed the localization and expression of Knl1, Bub1, and Mad2. No significant change in the abundance of Knl1 at kinetochores was observed in Wapl-depleted oocytes (fig. S6, A to C), and although the total levels of Bub1 and Mad2 were not affected by Wapl depletion, the abundance of both was decreased at kinetochores (fig. S6, D to J).

To precisely dissect Wapl interactions with Bub3, we purified recombinant full-length Bub3 and fragments of Wapl for in vitro binding assay (Fig. 5J). Bub3 could be pulled down by $Wapl_{1–300}$ but not the three other fragments ($Wapl_{301–600}$, $Wapl_{601–900}$, and $Wapl90_{1–1200}$) (Fig. 5K). This assay was further refined to document that $Wapl_{1–50}$, but not $Wapl_{51–300}$, bound to Bub3 (Fig. 5, L and M). Previous studies reported that the YSR motif in the N terminus of Wapl was required to mediate its binding to Pds5B or Haspin (*26*, *27*). Our co-IP data also showed that mutation of YSR motif to ASE (Y9A/R11E) in Wapl impaired its interaction with Bub3 (Fig. 5N) and that mutant Wapl cannot restore Bub3 and the accelerated meiotic progression caused by Wapl depletion (Fig. 5, O and P). Thus, it indicates that the interaction between Wapl and Bub3 is required for the maintenance of Bub3 protein level and SAC activity in oocyte meiosis.

To further elucidate the underlying mechanisms by which Wapl regulates Bub3, we evaluated mRNA levels of Bub3 upon Wapl depletion and found that Wapl did not affect the transcription of Bub3 (fig. S7A). We next explored the possibility that Wapl binding masks posttranslational modifications of Bub3, such as ubiquitination or sumoylation, to prevent its degradation. However, when we treated Wapl-depleted oocytes with the proteasome inhibitor MG132 or the sumoylation inhibitor ginkgolic acid, there was no significant increase of Bub3 (fig. S7B). In addition, overexpression of Wapl in oocytes did not increase the abundance of Bub3 (fig. S7C), suggesting that endogenous Wapl is sufficient to maintain Bub3 levels. Thus, Wapl regulates Bub3 through an unknown way that requires further investigation.

Elevation of Bub3 protein levels restores Wapl depletion–induced meiotic defects and aneuploidy

If reduced levels of Bub3 caused by depletion of Wapl cause meiotic defects and aneuploidy, then introduction of exogenous Bub3 into Wapl-depleted oocytes should reverse the phenotype. To test this hypothesis, we examined meiotic progression after microinjection of Bub3-HA mRNA into the Wapl-depleted oocytes (Bub3-rescue oocytes). Fluorescent imaging documented that Bub3-HA was correctly

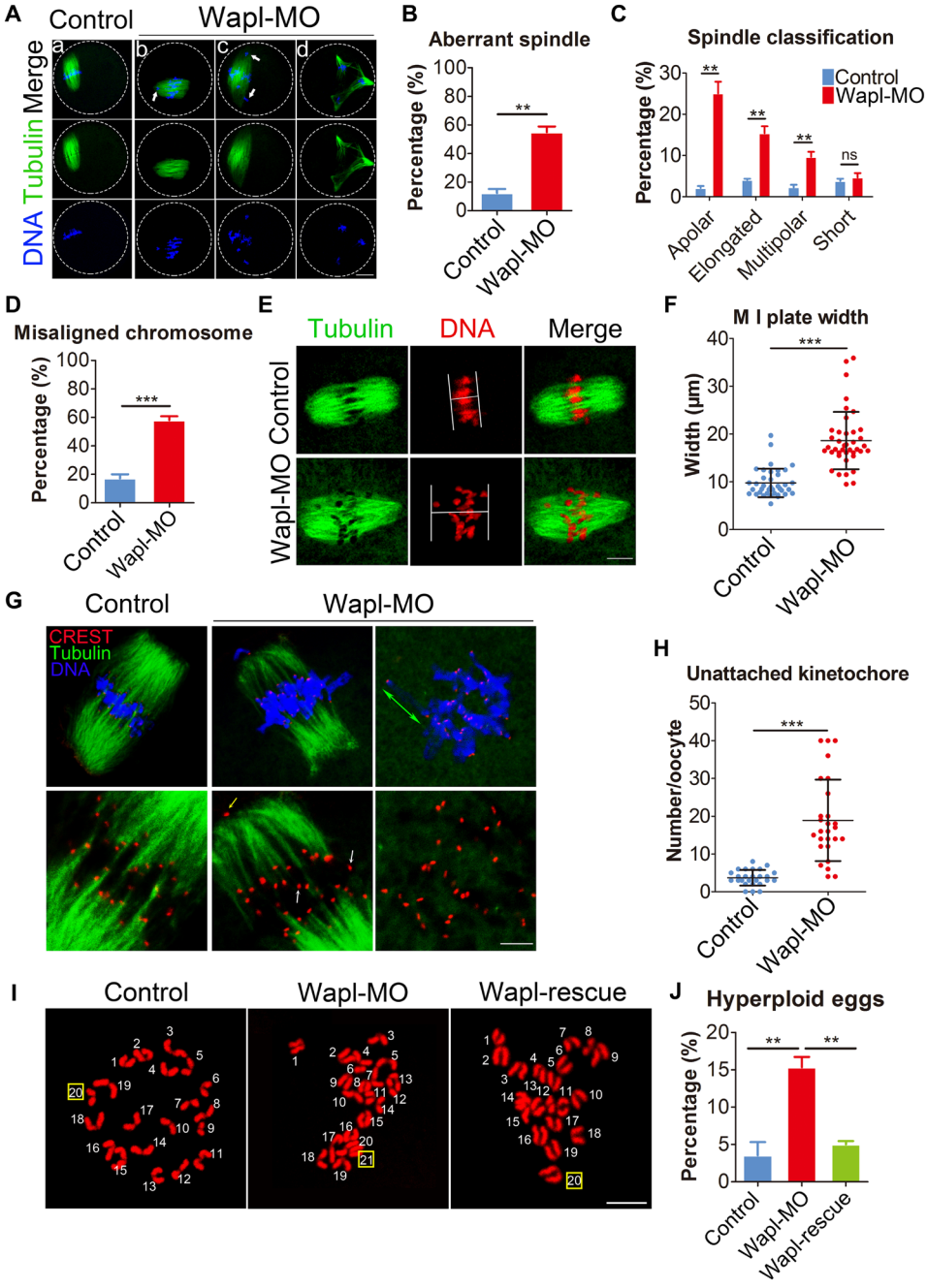

Fig. 3. Effect of Wapl depletion on the spindle assembly, chromosome alignment, K-MT attachment, and euploidy in mouse oocytes. (**A**) Representative images of spindle morphologies and chromosome alignment in control and Wapl-MO oocytes. GV oocytes were injected with control or Wapl-specific morpholinos, maintained for 20 hours in 2.5 μM milrinone before being washed into milrinone-free medium to allow resumption of meiosis. At 6 hours after GVBD, oocytes were fixed and immunostained for α-tubulin and DNA (Hoechst). Arrowheads indicate nonaligned bivalents. Scale bar, 20 μm. (**B**) The rate of abnormal spindles was recorded in control ($n = 102$) and Wapl-MO ($n = 108$) oocytes. (**C**) The rate of apolar, elongated, multipolar, and short spindles was recorded in control ($n = 102$) and Wapl-MO ($n = 108$) oocytes. (**D**) The rate of misaligned chromosomes was recorded in control ($n = 102$) and Wapl-MO ($n = 108$) oocytes. (**E**) Representative images of the width of M I plate in control and Wapl-MO oocytes. At 6 hours after GVBD, oocytes were fixed and immunostained for α-tubulin and DNA (PI). Scale bar, 10 μm. (**F**) The width of M I plate was measured in control ($n = 38$) and Wapl-MO ($n = 40$) oocytes. (**G**) Representative images of K-MT attachment in control and Wapl-MO oocytes. At 6 hours after GVBD, oocytes were incubated in M2 medium at 4°C for 10 min to induce the depolymerization of unstable microtubules and then immediately fixed and immunostained for α-tubulin, CREST, and DNA (Hoechst). White, yellow, and green arrows indicate nonconnected kinetochores, polar kinetochores, and stretched bivalents, respectively. Scale bar, 5 μm. (**H**) The number of unattached kinetochores was recorded in control ($n = 26$) and Wapl-MO ($n = 27$) oocytes. (**I**) Representative images of euploid and aneuploid M II eggs. Chromosome spreading was performed to count the number of chromosomes in control, Wapl-MO, and Wapl-rescue oocytes at 10 hours after GVBD. Scale bar, 5 μm. (**J**) The rate of hyperploid eggs was recorded in control ($n = 60$), Wapl-MO ($n = 60$), and Wapl-rescue ($n = 61$) oocytes. Data of (B) to (D) and (J) were presented as mean percentage (mean ± SEM) of at least three independent experiments. Data of (F) and (H) were presented as mean value (mean ± SD) of at least three independent experiments. $^{**}P < 0.01$, $^{***}P < 0.001$.

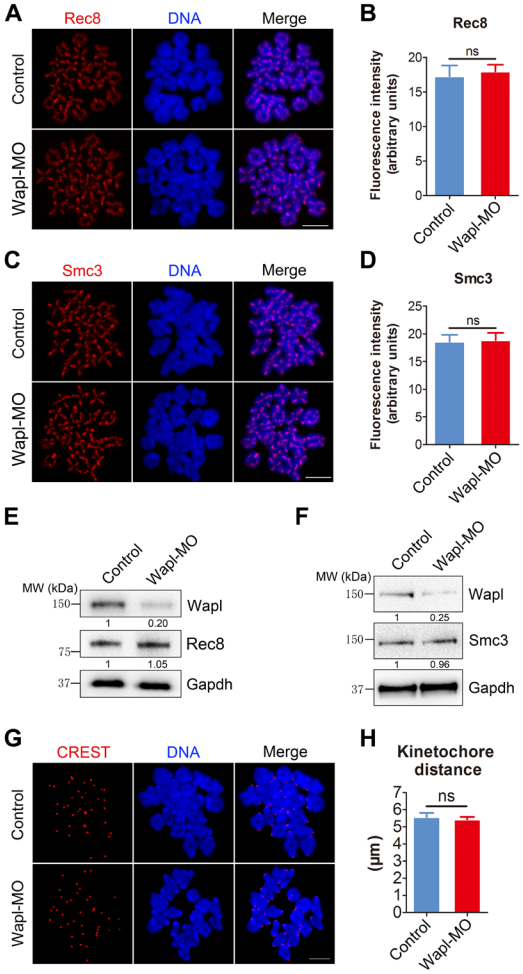

Fig. 4. Effect of Wapl depletion on cohesin binding. (**A**) Representative images of localization of Rec8 on the chromosomes in control and Wapl-MO oocytes. GV oocytes were injected with control or Wapl-specific morpholinos, maintained for 20 hours in 2.5 μM milrinone before being washed into milrinone-free medium to allow resumption of meiosis. At 6 hours after GVBD, oocytes immunostained for Rec8 and DNA (Hoechst) following chromosome spreading. Scale bar, 10 μm. (**B**) The fluorescence intensity of Rec8 was measured in control ($n = 200$, bivalents) and Wapl-MO ($n = 200$, bivalents) oocytes. (**C**) Representative images of localization of Smc3 on the chromosomes in control and Wapl-MO oocytes. GV oocytes were injected with control or Wapl-specific morpholinos, maintained for 20 hours in 2.5 μM milrinone before being washed into milrinone-free medium to allow resumption of meiosis. At 6 hours after GVBD, oocytes were immunostained for Smc3 and DNA (Hoechst) following chromosome spreading. Scale bar, 10 μm. (**D**) The fluorescence intensity of Smc3 was measured in control ($n = 200$, bivalents) and Wapl-MO ($n = 200$, bivalents) oocytes. (**E**) The protein levels of Rec8 were assessed by immunoblotting in control and Wapl-MO oocytes. Two hundred oocytes at 6 hours after GVBD for each group were collected and immunoblotted for Wapl, Rec8, and Gapdh. (**F**) The protein levels of Smc3 were assessed by immunoblotting in control and Wapl-MO oocytes. Two hundred oocytes at 6 hours after GVBD for each group were collected and immunoblotted for Wapl, Smc3, and Gapdh. (**G**) Representative images of bivalents and kinetochores in control and Wapl-MO oocytes. GV oocytes were injected with control or Wapl-specific morpholinos, maintained for 20 hours in 2.5 μM milrinone before being washed into milrinone-free medium to allow resumption of meiosis. At 6 hours after GVBD, oocytes were immunostained for CREST and DNA (Hoechst) following chromosome spreading. Scale bar, 10 μm. (**H**) The distance between kinetochore pairs within a bivalent was measured in control ($n = 200$, kinetochore pairs) and Wapl-MO ($n = 200$, kinetochore pairs) oocytes. Data of (B), (D), and (H) were presented as mean value (mean ± SEM) of at least three independent experiments.

located at kinetochores and immunoblot confirmed that levels of Bub3 were comparable to controls in Bub3-rescue oocytes (fig. S8, A and B). The accelerated PB1 extrusion at 6 and 7 hours after GVBD observed in Wapl-depleted oocytes reverted in Bub3-rescued oocytes to that of control oocytes (Fig. 6A). However, the Bub3QE (E213Q/K216E/K217E/K218E) mutant (*28*) that does not localize to the kinetochores was not able to correct the accelerated meiotic progression after expression in Wapl-depleted oocytes, although the protein level was normal (fig. S8, C to E). We also expressed exogenous Mad2, another core SAC component, in Wapl-depleted oocytes but did not observe the recovery of accelerated PB1 extrusion (fig. S8, F and G). In addition, the higher frequency of abnormal spindles, misaligned chromosomes, and incorrect K-MT attachments observed in Wapl-depleted oocytes was reduced to a level indistinguishable from controls in Bub3-rescue oocytes (Fig. 6, B, C, F, and G). In addition, the defective spindle length and width of chromosome plate at M I stage was restored in Bub3-rescue oocytes (Fig. 6, B, D, and E). Last, expression of exogenous Bub3 rescued the high incidence of aneuploidy exhibited in Wapl-depleted oocytes to comparable levels of control oocytes (Fig. 6, H and I). Collectively, these results indicate that recovery of Bub3 levels functionally rescues the defects caused by Wapl depletion, and the involvement of Wapl in the meiotic progression and control of the SAC is mediated by Bub3.

DISCUSSION

In eukaryotic cells, most cohesin complexes are stripped from chromosome arms during mitotic prophase and prometaphase in the "prophase pathway" mediated by Wapl (*29*). However, during meiosis, chromosome cohesion is established when DNA replication and recombination occur in fetal oocytes. After birth, during meiotic prophase, the homologous chromosomes become paired and joined by the process of homologous recombination to form a bivalent (*30*). Then, during meiosis I, cohesin complexes adhere to bivalents until the onset of anaphase I when the distal cohesin of bivalent arms is removed by cleavage of Rec8 by Separase (*23*, *31*–*33*). It is not known whether Wapl functions as a cohesin release factor to facilitate resolution of chiasmata by Separase, which prompted us to investigate its role during oocyte meiosis I.

Localization and expression patterns of Wapl differ during somatic cell mitosis and germ cell meiosis. In mitotic cells, Wapl is expressed throughout the cell cycle, but not present on chromosomes from prometaphase to anaphase (*12*). In sharp contrast, we observed up-regulation of Wapl expression during meiosis and accumulation on chromosomes, which suggested distinct functions. Unexpectedly, Wapl depletion accelerates meiotic progression in mouse oocytes as evidenced by premature extrusion of the first polar body. In contrast, depletion of Wapl delays the progression through the early stages of mitosis and more cells are arrested in prophase and prometaphase stages (*11*). Previous studies indicated that precocious PBE in oocytes is highly correlated with SAC dysfunction (*22*, *34*, *35*). In our studies, we find that the SAC activity is impaired and accompanied by various meiotic defects in Wapl-depleted oocytes including aberrant spindle assembly, improper chromosome alignment, and incorrect K-MT attachments that lead to aneuploidy. From these observations, we conclude that Wapl is required for SAC control and meiotic progression during meiosis I. These defects are not caused by the compromised cohesion because Wapl depletion does not affect the cohesin binding and bivalent resolution.

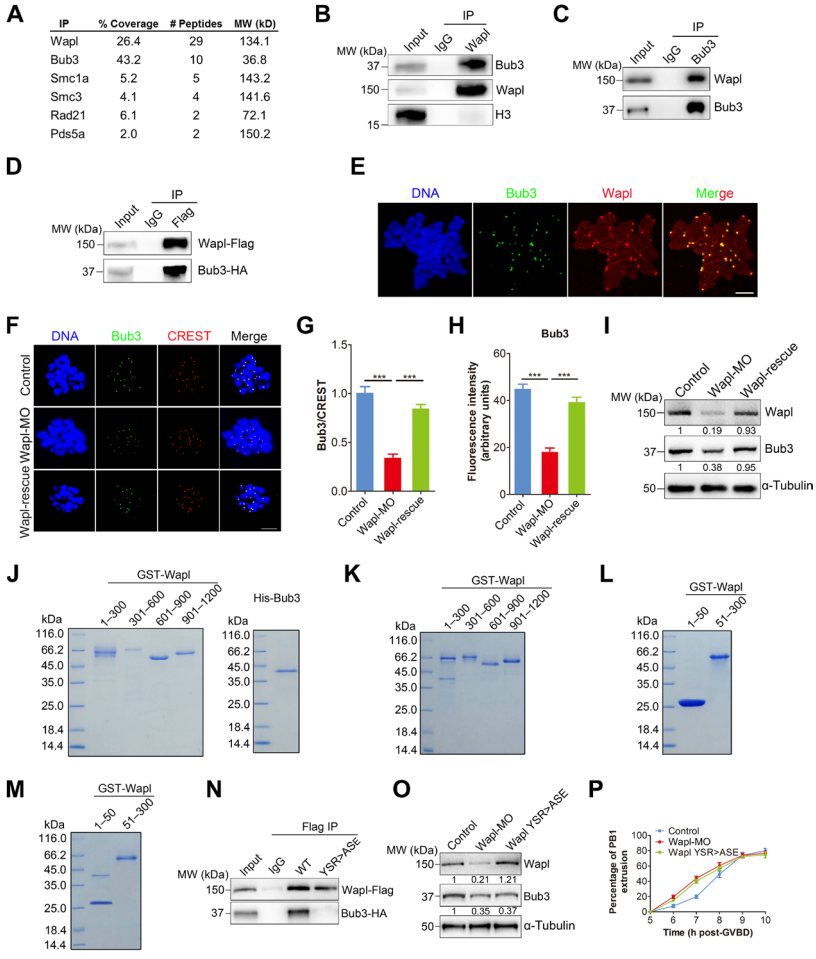

Fig. 5. The interaction between Wapl and Bub3. (**A**) Identification of binding partners of Wapl by immunoprecipitation and MS. The protein coverage, the number of peptides, and the molecular weight were shown for each molecule. (**B**) Co-IP was performed to determine the interaction between Wapl and Bub3. Oocytes were collected at 3 hours after GVBD (prometaphase I stage). Oocyte lysates were incubated with immunoglobulin G (IgG) and anti-Wapl antibody, respectively, followed by incubation with protein G beads. The blots of 5% of input and IP eluates were probed with anti-Bub3 and anti-Wapl antibodies, respectively. IP eluates were immunoblotted for histone H3 as a negative control. (**C**) Reciprocal co-IP was performed with IgG and anti-Bub3 antibody, respectively. The blots of 5% of input and IP eluates were probed with anti-Wapl and anti-Bub3 antibodies, respectively. (**D**) HEK293 cells were cotransfected with Wapl-Flag and Bub3-HA plasmids and subjected to co-IP using anti-Flag antibody. The interaction between Wapl-Flag and Bub3-HA was shown by the presence of Bub3-HA in the IP eluate pulled down by anti-Flag antibody. Five percent of input was used for immunoblotting. (**E**) Colocalization of Wapl with Bub3. At 3 hours after GVBD, oocytes were costained for Wapl and Bub3 following chromosome spreading. Scale bar, 5 μm. (**F**) Localization of Bub3 at prometaphase I stage in control, Wapl-MO, and Wapl-rescue oocytes. GV oocytes were injected with control or Wapl-specific morpholinos, maintained for 20 hours in 2.5 μM milrinone before being washed into milrinone-free medium to allow resumption of meiosis. For the rescue experiment, GV oocytes were injected with Wapl-specific morpholinos and maintained for 20 hours in 2.5 μM milrinone before being injected with Wapl mRNA and maintained for a further 2 hours in 2.5 μM milrinone to allow time for Wapl translation. Oocytes were then washed into milrinone-free medium to allow resumption of meiosis. At 3 hours after GVBD, oocytes were fixed and immunostained for Bub3, CREST, and DNA (Hoechst). Scale bar, 10 μm. (**G**) The relative fluorescence intensity of Bub3 to CREST was measured in control ($n = 189$), Wapl-MO ($n = 183$), and Wapl-rescue ($n = 171$) oocytes. The signal intensity of Bub3 was normalized with that of CREST. (**H**) The fluorescence intensity of Bub3 was measured in control ($n = 189$), Wapl-MO ($n = 183$), and Wapl-rescue ($n = 171$) oocytes. (**I**) The protein levels of Bub3 were detected by immunoblots of control, Wapl-MO, and Wapl-rescue oocytes. Two hundred oocytes at 3 hours after GVBD for each group were collected and immunoblotted for Wapl, Bub3, and α-tubulin. (**J**) Coomassie-stained SDS-polyacrylamide gel electrophoresis (PAGE) gel of the purified recombinant Wapl fragments and full-length Bub3. 1–300, $Wapl_{1–300}$; 301–600, $Wapl_{301–600}$; 601–900, $Wapl_{601–900}$; 901–1200, $Wapl_{901–1200}$. (**K**) Coomassie-stained SDS-PAGE gel of the recombinant Bub3 bound to the recombinant $Wapl_{1–300}$ fragment following glutathione *S*-transferase (GST) pull down. (**L**) Coomassie-stained SDS-PAGE gel of the purified recombinant Wapl fragments. 1–50, $Wapl_{1–50}$; 51–300, $Wapl_{51–300}$. (**M**) Coomassie-stained SDS-PAGE gel of the recombinant Bub3 bound to the recombinant $Wapl_{1–50}$ fragment following GST pull down. (**N**) HEK293 cells were cotransfected with wild-type (WT) or mutant (YSR>ASE) Wapl-Flag and Bub3-HA plasmids and then subjected to co-IP experiment using anti-Flag antibody. The interaction between Wapl-Flag and Bub3-HA was shown by the presence of Bub3-HA in the IP eluate pulled down by anti-Flag antibody. Ten percent of input was used for immunoblotting. (**O**) The protein levels of Bub3 were detected by immunoblotting in control, Wapl-MO, and mutant (YSR>ASE) Wapl-rescue oocytes. Two hundred oocytes at 3 hours after GVBD for each group were collected and immunoblotted for Wapl, Bub3, and α-tubulin. (**P**) Meiotic progression in control ($n = 113$), Wapl-MO ($n = 110$), and mutant (YSR>ASE) Wapl-rescue ($n = 108$) oocytes was shown by recording the rate of first PBE from 5 to 10 hours after GVBD. GV oocytes were injected with control or Wapl-specific morpholinos, maintained for 20 hours in 2.5 μM milrinone before being washed into milrinone-free medium to allow resumption of meiosis. For the rescue experiments, GV oocytes were injected with Wapl-specific morpholinos and maintained for 20 hours in 2.5 μM milrinone before being injected with mutant (YSR>ASE) Wapl mRNA and maintained for a further 2 hours in 2.5 μM milrinone to allow time for mutant Wapl translation. Oocytes were then washed into milrinone-free medium to allow resumption of meiosis. Data of (G), (H), and (P) were presented as mean value (mean ± SEM) of at least three independent experiments. ***$P < 0.001$.

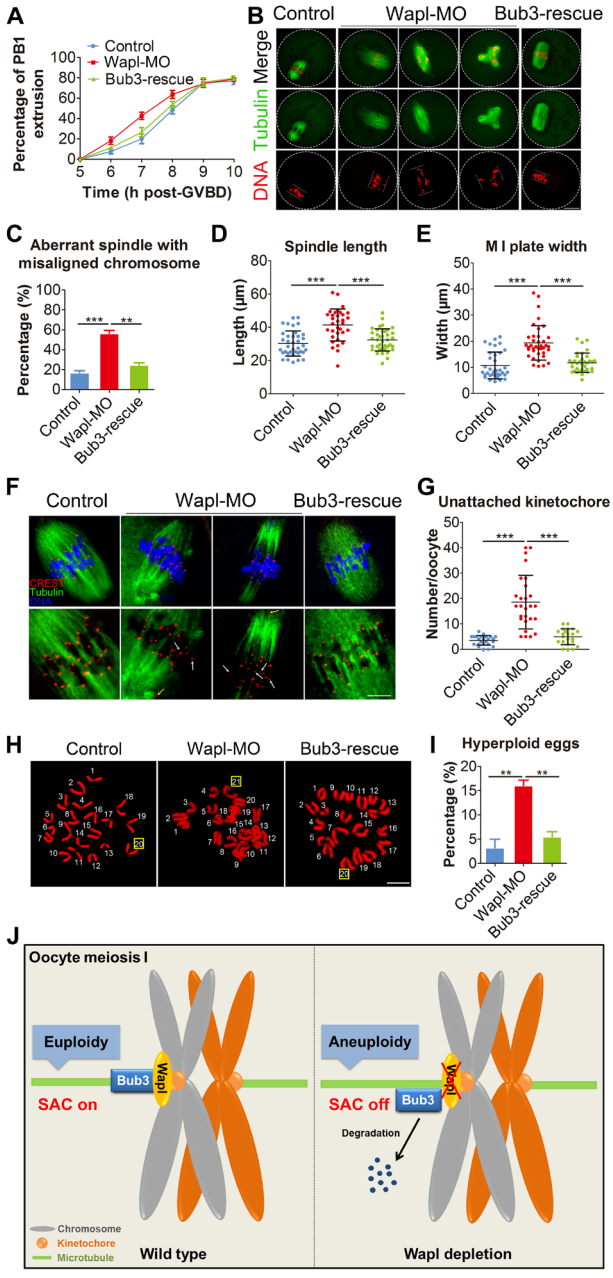

Fig. 6. Meiotic defects in Wapl-depleted oocytes could be restored by expression of exogenous Bub3. (**A**) Meiotic progression in control ($n = 135$), Wapl-MO ($n = 124$), and Bub3-rescue ($n = 115$) oocytes was determined by recording the rate of first PBE from 5 to 10 hours after GVBD. GV oocytes were injected with control or Wapl-specific morpholinos, maintained for 20 hours in 2.5 μM milrinone before being washed into milrinone-free medium to allow resumption of meiosis. For the rescue experiment, GV oocytes were injected with Wapl-specific morpholino and maintained for 20 hours in 2.5 μM milrinone before being injected with Bub3 mRNA and maintained for a further 2 hours in 2.5 μM milrinone to allow time for Bub3 translation. Oocytes were then washed into milrinone-free medium to allow resumption of meiosis. (**B**) Representative images of spindle morphologies and chromosome alignment in control, Wapl-MO, and Bub3-rescue oocytes. At 6 hours after GVBD, oocytes were fixed and immunostained for α-tubulin and DNA (PI). Scale bar, 20 μm. (**C**) Abnormal spindles with misaligned chromosomes were quantified in control ($n = 75$), Wapl-MO ($n = 82$), and Bub3-rescue ($n = 87$) oocytes. (**D**) The spindle length was measured in control ($n = 37$), Wapl-MO ($n = 33$), and Bub3-rescue ($n = 38$) oocytes at M I stage. (**E**) The width of M I plate was measured in control ($n = 36$), Wapl-MO ($n = 38$), and Bub3-rescue ($n = 35$) oocytes. (**F**) Representative images of K-MT attachment in control, Wapl-MO, and Bub3-rescued oocytes. At 6 hours after GVBD, oocytes were fixed and immunostained for α-tubulin, CREST, and DNA (Hoechst). White and yellow arrows indicate nonconnected kinetochores and polar kinetochores, respectively. Scale bar, 5 μm. (**G**) The rate of unattached kinetochores was recorded in control ($n = 25$), Wapl-MO ($n = 27$), and Bub3-rescue ($n = 22$) oocytes. (**H**) Representative images of euploid and aneuploid M II eggs. Chromosome spreading was performed to count the number of chromosomes in control, Wapl-MO, and Bub3-rescued oocytes at 10 hours after GVBD. Scale bar, 5 μm. (**I**) The rate of hyperploid eggs was recorded in control ($n = 66$), Wapl-MO ($n = 61$), and Bub3-rescue ($n = 59$) oocytes. Data of (A), (C), and (I) were presented as mean percentage (mean ± SEM) of at least three independent experiments. Data of (D), (E), and (G) were presented as mean value (mean ± SD) of at least three independent experiments. $^{**}P < 0.01$, $^{***}P < 0.001$. (**J**) Working model of how Wapl functions in control of the SAC during meiosis I. In normal oocytes, Wapl binds to and stabilizes Bub3 to maintain the SAC function, consequently ensuring euploid eggs. However, in oocytes depleted of Wapl, the SAC function is compromised due to the degradation of Bub3, resulting in aneuploid eggs.

The SAC certifies correct attachment of spindle microtubules to kinetochores and licenses cells to progress into anaphase to ensure accurate chromosome segregation (*25*). It was initially suggested that mammalian oocytes may not have a functional SAC because they can proceed through meiosis despite misaligned chromosomes, which results in higher rates of aneuploidy compared to somatic cells (*36*). Subsequent investigations documented that depletion of each SAC protein (Mps1, Bub1, BubR1, Bub3, Mad1, and Mad2) by knockdown or knockout unexceptionally resulted in an accelerated progression of meiosis I and an increased frequency of aneuploidy in mature oocytes (*22*, *34*, *37*–*40*), demonstrating that SAC is both present and functional in female germ cells. Our current findings document that Wapl participates in the SAC control to orchestrate meiotic progression and prevent aneuploidy in oocytes.

To further explore the molecular biology of Wapl in SAC control, we performed the immunoprecipitation of Wapl followed by MS to identify binding partners. A key member of the SAC complex, Bub3, was detected, and co-IP and in vitro binding experiments verified interaction between the two proteins. In oocyte meiosis I, the similar localization pattern of Wapl and Bub3 provides the prerequisite for their interaction. However, in mitotic cells, inhibitory factors might exist to prevent their binding. Thus, we hypothesized that Bub3 might be a downstream effector that mediates the participation of Wapl in the SAC control in oocytes. Bub3 protein is substantially reduced in Wapl-depleted oocytes, and expression of exogenous Bub3 restores the meiotic defects caused by Wapl depletion. These observations demonstrate that the involvement of Wapl in SAC control is mediated by Bub3.

This raises the key question of how Wapl affects the abundance of Bub3. We have ruled out Wapl regulation of Bub3 transcription and showed that inhibition of ubiquitination or sumoylation did not affect degradation of Bub3. It remains possible that Wapl acts as a molecular chaperone to facilitate Bub3 folding into a final compact and stable confirmation resistant to destruction (*41*). Increasing evidence has shown that cohesin subunits and regulators are implicated in biological processes in addition to chromosome cohesion. Our previous studies reported that cohesin establishment factors, Esco1 and Esco2, regulate distinct functions during oocyte meiosis. Esco1 acetylates α-tubulin to ensure microtubule stability to promote spindle assembly (*42*). Esco2 maintains H4K16 acetylation to participate in kinetochore functions for the SAC activity (*43*). In the current study, we find that cohesin release factor Wapl interacts with Bub3 to mediate the SAC function in oocyte meiosis I, which enriches our mechanistic understanding of the formation of aneuploid eggs (Fig. 6J). We demonstrate that, as two crucial regulators of cell cycle, cohesin and the SAC share common regulators to coordinate faithful chromosome segregation and orchestrate meiotic progression. One limitation of our present work is that we only assessed a short-term effect of Wapl depletion on the oocyte meiosis by knockdown approaches, and future studies will be conducted to evaluate the long-term effects of Wapl ablation on the oogenesis and oocyte development using a knockout mouse model.

MATERIALS AND METHODS

Animals

Four- to 6-week-old female ICR mice were used in all experiments, which were approved by the Animal Care and Use Committee of Nanjing Agricultural University, China and were performed in accordance with institutional guidelines.

Antibodies

Rabbit polyclonal anti-Wapl antibody was purchased from Bethyl Laboratories (Montgomery, TX, USA; catalog no. A300-268A-T); goat polyclonal anti-BubR1 antibody, rabbit polyclonal anti-Rec8 antibody, rabbit monoclonal anti-Smc3 antibody, rabbit monoclonal anti-Bub3 antibody, rabbit monoclonal anti-H3 antibody, rabbit polyclonal anti-Knl1 antibody, rabbit monoclonal anti-Bub1 antibody, rabbit monoclonal anti-Securin antibody, horseradish peroxidase (HRP)–conjugated goat anti-mouse immunoglobulin G (IgG) (H+L), and HRP-conjugated goat anti-rabbit IgG (H+L) were purchased from Abcam (Cambridge, MA, USA; catalog nos. ab28193, ab38372, ab128919, ab133699, ab176842, ab97023, ab70537, ab195268, ab79546, and ab97051); mouse monoclonal anti–α-tubulin–fluorescein isothiocyanate (FITC) antibody was purchased from Sigma (St. Louis, MO, USA; catalog no. F2168); human anti-centromere antibody was purchased from Antibodies Incorporated (Davis, CA, USA; catalog no. CA95617); mouse monoclonal anti-hemagglutinin (HA) antibody and Alexa Fluor 555–conjugated goat anti-human IgG (H+L) were purchased from Thermo Fisher Scientific (Waltham, MA, USA; catalog nos. 26183 and A-21433); rabbit monoclonal anti-Flag antibody and rabbit monoclonal anti-Gapdh (glyceraldehyde-3-phosphate dehydrogenase) antibody were purchased from Cell Signaling Technology (Danvers, MA, USA; catalog nos. 14793 and 2118); mouse monoclonal anti–α-tubulin antibody was purchased from Santa Cruz Biotechnology (Dallas, TA, USA; catalog no. sc-5286); and rabbit polyclonal anti-Mad2 antibody was purchased from Proteintech (Rosemont, IL, USA; catalog no. 10337-1-AP). Tetramethyl rhodamine isothiocyanate (TRITC)–conjugated goat anti-rabbit IgG (H+L) was purchased from Zhongshan Golden Bridge Biotechnology Co. Ltd. (Beijing, China).

Oocyte collection and culture

Female ICR mice were sacrificed by cervical dislocation. Fully grown oocytes arrested at prophase of meiosis I were collected from ovaries in M2 medium. Only those immature oocytes displaying a GV were cultured further in M16 medium under liquid paraffin oil at 37°C in an atmosphere of 5% CO_2 incubator for in vitro maturation. At different time points after culture, oocytes were collected for subsequent analysis.

Morpholino knockdown

Wapl-targeting morpholino antisense oligo (Gene Tools, Philomath, OR, USA; 5′-TCTGGATGTCATTTTGACACCTGTT-3′) was diluted with water to provide a working concentration of 1 mM, and then approximately 5 to 10 pl of oligo were microinjected into the cytoplasm of fully grown GV oocytes using a Narishige microinjector (Tokyo, Japan). A nontargeting morpholino oligo (5′-CCTCTTACCTCAGT-TACAATTTATA-3′) was injected as a control. To facilitate the morpholino-mediated inhibition of mRNA translation, oocytes were arrested at GV stage in M16 medium containing 2.5 μM milrinone for 20 hours and then cultured in milrinone-free M16 medium for subsequent experiments.

siRNA knockdown

Wapl-targeting siRNA oligo (GenePharma, Shanghai, China; antisense sequence: 5′-UUCUUUGCCUGAUUCAGGCTT-3′) was diluted with water to provide a working concentration of 25 μM, and then approximately 5 to 10 pl of oligo were microinjected into the cytoplasm of fully grown GV oocytes using a Narishige microinjector (Tokyo, Japan). A nontargeting siRNA oligo (antisense sequence:

5′-ACGUGACACGUUCGGAGAATT-3′) was injected as a control. To facilitate the degradation of mRNA by siRNA, oocytes were arrested at GV stage in M16 medium containing 2.5 μM milrinone for 24 hours and then transferred to milrinone-free M16 medium to resume the meiosis for subsequent experiments.

mRNA construct and in vitro transcription

Mouse wild-type (WT) Wapl complementary DNA (cDNA) was subcloned into pcDNA3.1/GFP or pcDNA3.1/Flag vectors. Mutant Wapl with four silent third-codon point mutations in the sequence targeted by the morpholino provided a MO-resistant construct. Mutant Wapl with three silent third-codon point mutations in the sequence targeted by the seed region of siRNA antisense strand provided a siRNA-resistant construct. Y9A/R11E mutations in Wapl were created for YSR>ASE mutant. All point mutations were introduced with the GeneArt Site-Directed Mutagenesis PLUS System (Thermo Fisher Scientific, Waltham, MA, USA). WT mouse Bub3 cDNA was subcloned into pcDNA3.1/HA vector. E213Q/K216E/K217E/K218E mutations in Bub3 were created for Bub3QE mutant. Capped mRNA was synthesized from linearized plasmid using a T7 mMessage mMachine kit (Thermo Fisher Scientific, Waltham, MA, USA) and purified with a MEGAclear kit (Thermo Fisher Scientific, Waltham, MA, USA). Typically, 10 to 12 pl of mRNA (0.5 to 1.0 μg/μl) were injected into oocytes and then arrested at the GV stage in M16 medium containing 2.5 μM milrinone for 2 hours, allowing enough time for translation, followed by releasing into milrinone-free M16 medium for further study.

Immunofluorescence and confocal microscopy

Oocytes were fixed in 4% paraformaldehyde in phosphate-buffered saline (PBS) (pH 7.4) for 30 min and permeabilized in 0.5% Triton X-100 for 20 min at room temperature. Then, oocytes were blocked with 1% bovine serum albumin (BSA)–supplemented PBS for 1 hour and incubated with anti-Wapl (1:100), anti-Rec8 (1:100), anti-Smc3 (1:100), anti-Bub3 (1:200), anti-BubR1 (1:100), anti-Knl1 (1:100), anti-Bub1 (1:100), anti-Mad2 (1:50), anti–α-tubulin-FITC (1:300), or anti-centromere (1:200) antibodies at 4°C overnight. After washing in phosphate-buffered saline with Tween 20 (PBST), oocytes were incubated with an appropriate secondary antibody for 1 hour at room temperature. Then, oocytes were counterstained with propidium iodide (PI) or Hoechst for 10 min. Last, oocytes were mounted on glass slides and observed under a confocal microscope (Carl Zeiss 700).

For measurement of fluorescence intensity, the signals from both control and treatment oocytes were acquired by performing the same immunostaining procedure and setting up the same parameters for confocal microscopy. The average fluorescence intensity per unit area within the region of interest was applied to quantify the fluorescence of each oocyte images. Fluorescence intensity was randomly measured by plot profiling using ImageJ software (National Institutes of Health, USA). Fluorescence intensity on kinetochores was quantified by drawing a circle of the dot-like CREST staining that includes SAC protein staining. The intensity of SAC proteins was normalized against the CREST fluorescence intensity.

Immunoprecipitation and immunoblots

Immunoprecipitation was carried out using 20 ovaries or 800 oocytes according to the instructions for ProFound Mammalian Co-Immunoprecipitation Kit (Thermo Fisher Scientific, Waltham, MA, USA). For immunoblots, 200 oocytes were lysed in 4× lithium dodecyl sulfate (LDS) sample buffer (Thermo Fisher Scientific, Waltham, MA, USA) containing protease inhibitor and then separated on 10% bis-tris precast gels and transferred onto polyvinylidene difluoride membranes. The blots were blocked in tris-buffered saline with Tween 20 (TBST) containing 5% low-fat dry milk for 1 hour at room temperature and then incubated with anti-Wapl (1:1000), anti-Bub3 (1:1000), anti-Rec8 (1:1000), anti-Smc3 (1:1000), anti-Flag (1:1000), anti-HA (1:1000), anti-Securin (1:2000), anti-BubR1 (1:500), anti-Bub1 (1:1000), anti-Mad2 (1:500), anti–α-tubulin (1:5000), or anti-Gapdh (1:5000) antibodies overnight at 4°C. After washing in TBST, the blots were incubated with HRP-conjugated secondary antibodies for 1 hour at room temperature. Chemiluminescence was detected with ECL Plus (GE, Piscataway, NJ, USA), and protein bands were acquired using the Tanon 3900 Chemiluminescence Imaging System. Images with different exposure times for each blot were acquired, and one without underexposure as well as overexposure was selected as the final data. Band intensities were quantified using ImageJ software and normalized to loading controls. The original blots were shown in the Supplementary Materials (figs. S9 and S10).

Liquid chromatography–MS/MS and data analysis

The peptide samples were dissolved in 2% acetonitrile/0.1% formic acid and analyzed using TripleTOF 5600+ MS coupled with the Eksigent nanoLC System (SCIEX, USA). Peptide was loaded onto a C18 trap column (5 μm, 100 μm × 20 mm), and eluted at 300 nl/min onto a C18 analytical column (3 μm, 75 μm × 150 mm) over a 60-min gradient. The two mobile phases were buffer A (2% acetonitrile/0.1% formic acid/98% H_2O) and buffer B (98% acetonitrile/0.1% formic acid/2% H_2O). For IDA (information-dependent acquisition), survey scans were acquired in 250 ms, and 40 product ion scans were collected in 50 ms/per scan. MS1 spectra were collected in the range of 350 to 1500 mass/charge ratio (m/z), and MS2 spectra were collected in the range of 100 to 1500 m/z. Precursor ions were excluded from reselection for 15 s.

Protein identification was achieved by searching the obtained MS spectra files using software ProteinPilot 4.5 Software (July 2012; AB Sciex) against a database from UniProt mouse protein sequencing data. All identified proteins had an Unused Protscore of >1.3 (which corresponds to proteins identified with >95% confidence), and proteins with one unique peptide were considered confidently identified.

In vitro binding assay

Various truncation fragments of mouse Wapl were constructed with the PGEX-4T-1 vector to produce glutathione *S*-transferase (GST) fusion proteins, which were expressed in *Escherichia coli* and purified with Glutathione Sepharose High Performance resin (GE, Piscataway, NJ, USA). Full-length mouse Bub3 was constructed with the pCzn1 vector to produce His-tagged fusion protein, which was expressed in *E. coli* and purified with the Ni Sepharose High Performance affinity resin (GE, Piscataway, NJ, USA). Standard GST pull-down assays were used to assess the binding of Wapl fragments to Bub3 in vitro. Briefly, purified GST-Wapl fragments and His-Bub3 were mixed and incubated at 4°C for 2 hours. Glutathione resin was then added to the mixture with end-over-end rotation at 4°C for 2 hours. Eluates from the resin were analyzed by SDS–polyacrylamide gel electrophoresis (PAGE) and Coomassie blue staining.

Chromosome spreading

Oocytes were incubated in Tyrode's buffer (pH 2.5) for about 30 s at 37°C to remove zona pellucidae. After recovery in M2 medium for

10 min, oocytes were fixed in a drop of 1% paraformaldehyde with 0.15% Triton X-100 on a glass slide. After air drying, chromosomes were counterstained with PI and examined by confocal microscopy.

Statistical analysis

All percentages or values from at least three repeated experiments were expressed as mean ± SEM or mean ± SD, and the number of oocytes observed was labeled in parentheses as (n). Data were analyzed by paired-samples t test, provided by GraphPad Prism5 statistical software. The level of significance was accepted as $P < 0.05$.

SUPPLEMENTARY MATERIALS

Supplementary material for this article is available at http://advances.sciencemag.org/cgi/content/full/6/15/eaax3969/DC1

View/request a protocol for this paper from *Bio-protocol*.

REFERENCES AND NOTES

1. B. Xiong, J. L. Gerton, Regulators of the cohesin network. *Annu. Rev. Biochem.* **79**, 131–153 (2010).
2. I. Sumara, E. Vorlaufer, P. T. Stukenberg, O. Kelm, N. Redemann, E. A. Nigg, J. M. Peters, The dissociation of cohesin from chromosomes in prophase is regulated by Polo-like kinase. *Mol. Cell* **9**, 515–525 (2002).
3. J. H. Haarhuis, A. M. Elbatsh, B. D. Rowland, Cohesin and its regulation: On the logic of X-shaped chromosomes. *Dev. Cell* **31**, 7–18 (2014).
4. V. P. Singh, J. L. Gerton, Cohesin and human disease: Lessons from mouse models. *Curr. Opin. Cell Biol.* **37**, 9–17 (2015).
5. R. Ciosk, M. Shirayama, A. Shevchenko, T. Tanaka, A. Toth, A. Shevchenko, K. Nasmyth, Cohesin's binding to chromosomes depends on a separate complex consisting of Scc2 and Scc4 proteins. *Mol. Cell* **5**, 243–254 (2000).
6. R. M. Alomer, E. M. L. da Silva, J. Chen, K. M. Piekarz, K. McDonald, C. G. Sansam, C. L. Sansam, S. Rankin, Esco1 and Esco2 regulate distinct cohesin functions during cell cycle progression. *Proc. Natl. Acad. Sci. U.S.A.* **114**, 9906–9911 (2017).
7. T. Nishiyama, R. Ladurner, J. Schmitz, E. Kreidl, A. Schleiffer, V. Bhaskara, M. Bando, K. Shirahige, A. A. Hyman, K. Mechtler, J. M. Peters, Sororin mediates sister chromatid cohesion by antagonizing Wapl. *Cell* **143**, 737–749 (2010).
8. T. Nishiyama, M. M. Sykora, H. I. T. V. Pj, K. Mechtler, J. M. Peters, Aurora B and Cdk1 mediate Wapl activation and release of acetylated cohesin from chromosomes by phosphorylating Sororin. *Proc. Natl. Acad. Sci. U.S.A.* **110**, 13404–13409 (2013).
9. H. Liu, S. Rankin, H. Yu, Phosphorylation-enabled binding of SGO1-PP2A to cohesin protects sororin and centromeric cohesion during mitosis. *Nat. Cell Biol.* **15**, 40–49 (2013).
10. I. C. Waizenegger, J. F. Giménez-Abián, D. Wernic, J. M. Peters, Regulation of human separase by securin binding and autocleavage. *Curr. Biol.* **12**, 1368–1378 (2002).
11. S. Kueng, B. Hegemann, B. H. Peters, J. J. Lipp, A. Schleiffer, K. Mechtler, J. M. Peters, Wapl controls the dynamic association of cohesin with chromatin. *Cell* **127**, 955–967 (2006).
12. R. Gandhi, P. J. Gillespie, T. Hirano, Human Wapl is a cohesin-binding protein that promotes sister-chromatid resolution in mitotic prophase. *Curr. Biol.* **16**, 2406–2417 (2006).
13. A. Tedeschi, G. Wutz, S. Huet, M. Jaritz, A. Wuensche, E. Schirghuber, I. F. Davidson, W. Tang, D. A. Cisneros, V. Bhaskara, Wapl is an essential regulator of chromatin structure and chromosome segregation. *Nature* **501**, 564–568 (2013).
14. M. Petronczki, M. F. Siomos, K. Nasmyth, Un ménage à quatre: The molecular biology of chromosome segregation in meiosis. *Cell* **112**, 423–440 (2003).
15. K. De, L. Sterle, L. Krueger, X. Yang, C. A. Makaroff, Arabidopsis thaliana WAPL is essential for the prophase removal of cohesin during meiosis. *PLOS Genet.* **10**, e1004497 (2014).
16. K. Challa, M. S. Lee, M. Shinohara, K. P. Kim, A. Shinohara, Rad61/Wpl1 (Wapl), a cohesin regulator, controls chromosome compaction during meiosis. *Nucleic Acids Res.* **44**, 3190–3203 (2016).
17. O. Crawley, C. Barroso, S. Testori, N. Ferrandiz, N. Silva, M. Castellano-Pozo, A. L. Jaso-Tamame, E. Martinez-Perez, Cohesin-interacting protein WAPL-1 regulates meiotic chromosome structure and cohesion by antagonizing specific cohesin complexes. *eLife* **5**, e10851 (2016).
18. M. Kuroda, K. Oikawa, T. Ohbayashi, K. Yoshida, K. Yamada, J. Mimura, Y. Matsuda, Y. Fujii-Kuriyama, K. Mukai, A dioxin sensitive gene, mammalian *WAPL*, is implicated in spermatogenesis. *FEBS Lett.* **579**, 167–172 (2005).
19. J. Zhang, H. Håkansson, M. Kuroda, L. Yuan, Wapl localization on the synaptonemal complex, a Meiosis-specific proteinaceous structure that binds homologous chromosomes, in the female mouse. *Reprod. Domest. Anim.* **43**, 124–126 (2008).
20. M. A. Brieño-Enríquez, S. L. Moak, M. Toledo, J. J. Filter, S. Gray, J. L. Barbero, P. E. Cohen, J. K. Holloway, Cohesin removal along the chromosome arms during the first meiotic division depends on a NEK1-PP1γ-WAPL axis in the mouse. *Cell Rep.* **17**, 977–986 (2016).
21. H. Homer, L. Gui, J. Carroll, A spindle assembly checkpoint protein functions in prophase I arrest and prometaphase progression. *Science* **326**, 991–994 (2009).
22. S. A. Touati, E. Buffin, D. Cladière, K. Hached, C. Rachez, J. M. van Deursen, K. Wassmann, Mouse oocytes depend on BubR1 for proper chromosome segregation but not for prophase I arrest. *Nat. Commun.* **6**, 6946 (2015).
23. K. T. Jones, S. I. Lane, Molecular causes of aneuploidy in mammalian eggs. *Development* **140**, 3719–3730 (2013).
24. S. I. Lane, Y. Yun, K. T. Jones, Timing of anaphase-promoting complex activation in mouse oocytes is predicted by microtubule-kinetochore attachment but not by bivalent alignment or tension. *Development* **139**, 1947–1955 (2012).
25. A. L. Marston, K. Wassmann, Multiple duties for spindle assembly checkpoint kinases in meiosis. *Front. Cell Dev. Biol.* **5**, 109 (2017).
26. C. Liang, Q. Chen, Q. Yi, M. Zhang, H. Yan, B. Zhang, L. Zhou, Z. Zhang, F. Qi, S. Ye, F. Wang, A kinase-dependent role for Haspin in antagonizing Wapl and protecting mitotic centromere cohesion. *EMBO Rep.* **19**, 43–56 (2017).
27. Z. Ouyang, G. Zheng, D. R. Tomchick, X. Luo, H. Yu, Structural basis and IP6 requirement for Pds5-dependent cohesin dynamics. *Mol. Cell* **62**, 248–259 (2016).
28. S. Zhu, R. Jing, Y. Yang, Y. Huang, X. Wang, Y. Leng, J. Xi, G. Wang, W. Jia, J. Kang, A motif from Lys216 to Lys222 in human BUB3 protein is a nuclear localization signal and critical for BUB3 function in mitotic checkpoint. *J. Biol. Chem.* **290**, 11282–11292 (2015).
29. I. C. Waizenegger, S. Hauf, A. Meinke, J. M. Peters, Two distinct pathways remove mammalian cohesin from chromosome arms in prophase and from centromeres in anaphase. *Cell* **103**, 399–410 (2000).
30. S. Burkhardt, M. Borsos, A. Szydlowska, J. Godwin, S. A. Williams, P. E. Cohen, T. Hirota, M. Saitou, K. Tachibanakonwalski, Chromosome cohesion established by Rec8-cohesin in fetal oocytes is maintained without detectable turnover in oocytes arrested for months in mice. *Curr. Biol.* **26**, 678–685 (2016).
31. S. A. Touati, K. Wassmann, How oocytes try to get it right: Spindle checkpoint control in meiosis. *Chromosoma* **125**, 321–335 (2016).
32. N. R. Kudo, K. Wassmann, M. Anger, M. Schuh, K. G. Wirth, H. Xu, W. Helmhart, H. Kudo, M. Mckay, B. Maro, Resolution of chiasmata in oocytes requires separase-mediated proteolysis. *Cell* **126**, 135–146 (2006).
33. N. R. Kudo, M. Anger, A. H. Peters, O. Stemmann, H. C. Theussl, W. Helmhart, H. Kudo, C. Heyting, K. Nasmyth, Role of cleavage by separase of the Rec8 kleisin subunit of cohesin during mammalian meiosis I. *J. Cell Sci.* **122**, 2686–2698 (2009).
34. B. E. Mcguinness, M. Anger, A. Kouznetsova, A. M. Gil-Bernabé, W. Helmhart, N. R. Kudo, A. Wuensche, S. Taylor, C. Hoog, B. Novak, Regulation of APC/C activity in oocytes by a Bub1-dependent spindle assembly checkpoint. *Curr. Biol.* **19**, 369–380 (2009).
35. Y. Qu, D. Lu, H. Jiang, X. Chi, H. Zhang, EZH2 is required for mouse oocyte meiotic maturation by interacting with and stabilizing spindle assembly checkpoint protein BubRI. *Nucl. Acids Res.* **44**, 7659–7672 (2016).
36. J. E. Holt, S. I. Lane, K. T. Jones, The control of meiotic maturation in mammalian oocytes. *Curr. Top. Dev. Biol.* **102**, 207–226 (2013).
37. K. Hached, S. Z. Xie, E. Buffin, D. Cladiere, C. Rachez, M. Sacras, P. K. Sorger, K. Wassmann, Mps1 at kinetochores is essential for female mouse meiosis I. *Development* **138**, 2261–2271 (2011).
38. M. Li, S. Li, J. Yuan, Z. B. Wang, S. C. Sun, H. Schatten, Q. Y. Sun, Bub3 is a spindle assembly checkpoint protein regulating chromosome segregation during mouse oocyte meiosis. *PLOS ONE* **4**, e7701 (2009).
39. T. Niault, K. Hached, R. Sotillo, P. K. Sorger, B. Maro, R. Benezra, K. Wassmann, Changing Mad2 levels affects chromosome segregation and spindle assembly checkpoint control in female mouse meiosis I. *PLOS ONE* **2**, e1165 (2007).
40. D. Zhang, M. Li, W. Ma, Y. Hou, Y. H. Li, S. W. Li, Q. Y. Sun, W. H. Wang, Localization of mitotic arrest deficient 1 (MAD1) in mouse oocytes during the first meiosis and its functions as a spindle checkpoint protein. *Biol. Reprod.* **72**, 58–68 (2005).
41. B. Bukau, A. L. Horwich, The Hsp70 and Hsp60 chaperone machines. *Cell* **92**, 351–366 (1998).
42. Y. Lu, S. Li, Z. Cui, X. Dai, M. Zhang, Y. Miao, C. Zhou, X. Ou, B. Xiong, The cohesion establishment factor Esco1 acetylates α-tubulin to ensure proper spindle assembly in oocyte meiosis. *Nucleic Acids Res.* **46**, 2335–2346 (2018).
43. Y. Lu, X. Dai, M. Zhang, Y. Miao, C. Zhou, Z. Cui, B. Xiong, Cohesin acetyltransferase Esco2 regulates SAC and kinetochore functions via maintaining H4K16 acetylation during mouse oocyte meiosis. *Nucleic Acids Res.* **45**, 9388–9397 (2017).

Acknowledgments

Funding: This work was supported by the National Natural Science Foundation of China (31822053), the National Key Research and Development Program of China (2018YFC1004002

and 2018YFC1003802), and the Fundamental Research Funds for the Central Universities (KJYQ201901). **Author contributions:** B.X. designed the research. C.Z., Y.M., Z.C., X.S., and Y.Z. performed the experiments. C.Z. and B.X. analyzed the data. C.Z. and B.X. wrote the manuscript. **Competing interests:** The authors declare that they have no competing interests. **Data and materials availability:** All data needed to evaluate the conclusions in the paper are present in the paper and/or the Supplementary Materials. Additional data related to this paper may be requested from the authors.

Submitted 19 March 2019
Accepted 14 January 2020
Published 8 April 2020
10.1126/sciadv.aax3969

Citation: C. Zhou, Y. Miao, Z. Cui, X. ShiYang, Y. Zhang, B. Xiong, The cohesin release factor Wapl interacts with Bub3 to govern SAC activity in female meiosis I. *Sci. Adv.* **6**, eaax3969 (2020).